www.lajss.org
Latin American Journal of Solids and Structures 3 (2006) 301–324

Numerical investigation of the flow in a two-dimensional cavity: meshless, finite volumes and finite differences methods

Antônio Carlos Henriques Marques and José Laércio Doricio

Departamento de Engenharia de Materiais,
Aeronáutica e Automobilística, EESC, USP,
São Carlos, SP, Brazil

Abstract

This study compares the Finite Volumes, Finite Differences and Meshless methods applied to the classic square driven cavity problem. It gives a brief exposition of the driven cavity flow problem, the scientific motivation of this study, the approach employed, and the goals to be achieved. The projection method was used to solve the Navier-Stokes equations. A structured mesh was employed for the Finite Differences method and an unstructured mesh for the Finite Volumes method. Cell centered was used for the velocity field $\mathbf{u}$ and the pressure field p in the Finite Volumes method. The convergence was accelerated through the Bi-conjugated Gradient Stabilized method. The necessary points to the Meshless method were obtained from the computational nodes generated by the Finite Volumes mesh. The exponential weight function and the Least Square method was used in the Meshless method. The primitive variables were adopted in all the formulations and Reynolds numbers 0.1, 10, 50 and 100 were used. The formulations are second order in spatial variables and first order explicit in time variables. Interesting characteristics of the flow are presented in details - the velocity field in the central lines and the streamlines. The results are listed in tables and the primary vortex position is compared with other authors. The Finite Volumes, Meshless and Finite Differences methods are compared and the errors among them are presented and discussed.

Keywords: finite volumes, finite differences, meshless, primitive variables, numerical simulation.

1 Introduction

The driven cavity flow has been studied very extensively in the literature. Driven cavity flow serves as a benchmark problem and almost every new numerical method for the 2-D steady incompressible Navier-Stokes equations is tested on the driven cavity in terms of accuracy, numerical efficiency, boundary conditions, etc. Reference [26] developed experimental techniques covering Reynolds numbers between 20 and 4000. Reference [16, 17] conducted experiments in

*Corresp. author email: josedoricio@yahoo.com.br Received 12 Jun 2006; In revised form 18 Aug 2006

a three-dimensional lid-driven cavity to study the effects of the end walls on the size of the downstream secondary edge.

Many authors used the driven cavity problem to validate schemes and numerical techniques. Reference [31] presented numerical techniques for solving problems of steady viscous incompressible flow in the plane, and used to obtain solutions for the driven cavity for Reynolds numbers between 1 and 10000.

Numerical formulations had been tested, by many authors, using the driven cavity problem, like streamfunction-vorticity [1]; streamfunction-velocity [14]; velocity-vorticity [21]; finite volume method for the vorticity-velocity equations [27]; high order compact method for the incompressible Navier-Stokes solutions [28]; sinc-collocation elements [24]; streamfunction-vorticity with SOR, fine grid mesh for Reynolds numbers until 20000 [7]. Books in fluid dynamics use the example of the driven cavity problem to show techniques and solutions of numerical and computational methods [34].

The square driven cavity problem is solved, in this paper, employing the incompressible Navier-Stokes equations [9]. These equations can be discretized using the Finite Volumes method for unstructured mesh - [19, 20, 29, 30], the Finite Differences method for structured mesh - [8, 20, 32, 34] - and the Meshless method for random points - [3, 6, 13, 22].

The main purpose of this study is to compare the Finite Volumes, Finite Differences and Meshless methods, applied to the driven cavity problem, analyzing the numerical accuracy and the boundary condition problems. The incompressible Navier-Stokes equations and the projection method [15] were used by all formulations for Re = 0.1, 10, 50 and 100. A brief discussion on the physical, mathematical and numerical nature of a 2-D driven cavity problem is also given.

2 Governing equations

The driven cavity problem is solved employing the incompressible Navier-Stokes equations to modeling the fluid dynamics phenomena. As for the numerical methods to solve the governing equations, the Finite Differences and Meshless methods use the differential formulation and the Finite Volumes method uses the integral formulation.

A solution for the incompressible Navier-Stokes equation system can be performed by two most common strategies: using the vorticity stream-function approach or the primitive variable approach. In this study, the primitive variable approach was adopted. The differential

formulation for the two-dimensional incompressible Navier-Stokes is given by:

$$\begin{cases} \dfrac{\partial u}{\partial t} + u\dfrac{\partial u}{\partial x} + v\dfrac{\partial u}{\partial y} = -\dfrac{\partial p}{\partial x} + \dfrac{1}{Re}\left(\dfrac{\partial^2 u}{\partial x^2} + \dfrac{\partial^2 u}{\partial y^2}\right) , \\ \dfrac{\partial v}{\partial t} + u\dfrac{\partial v}{\partial x} + v\dfrac{\partial v}{\partial y} = -\dfrac{\partial p}{\partial y} + \dfrac{1}{Re}\left(\dfrac{\partial^2 v}{\partial x^2} + \dfrac{\partial^2 v}{\partial y^2}\right) , \\ \dfrac{\partial u}{\partial x} + \dfrac{\partial v}{\partial y} = 0 . \end{cases} \tag{1}$$

where Re is the Reynolds number defined as $Re = \frac{\rho U_\infty L_\infty}{\nu}$, ρ is the density of the fluid, L_∞ and U_∞ are length and velocity characteristic of the flow, ν is the viscosity of the fluid; $\mathbf{u} = (u, v)$ is the velocity field and p is the pressure field.

Equation (1), in the conservative form, integrated in a control volume V gives:

$$\begin{cases} \displaystyle\int_V \frac{\partial u}{\partial t} dV = -\int_V \frac{\partial p}{\partial x} dV + \int_V \left[\frac{1}{Re}\left(\frac{\partial^2 u}{\partial x^2} + \frac{\partial^2 u}{\partial y^2}\right) - \frac{\partial u^2}{\partial x} - \frac{\partial uv}{\partial y}\right] dV , \\ \displaystyle\int_V \frac{\partial v}{\partial t} dV = -\int_V \frac{\partial p}{\partial y} dV + \int_V \left[\frac{1}{Re}\left(\frac{\partial^2 v}{\partial x^2} + \frac{\partial^2 v}{\partial y^2}\right) - \frac{\partial uv}{\partial x} - \frac{\partial v^2}{\partial y}\right] dV , \\ \displaystyle\int_V \left(\frac{\partial u}{\partial x} + \frac{\partial v}{\partial y}\right) dV = 0 . \end{cases} \tag{2}$$

Equation (2) can be written as:

$$\begin{cases} \displaystyle\int_V \frac{\partial u}{\partial t} dV = -\int_V \frac{\partial p}{\partial x} dV + \int_V \left[\frac{\partial}{\partial x}\left(\frac{1}{Re}\frac{\partial u}{\partial x} - u^2\right) + \frac{\partial}{\partial y}\left(\frac{1}{Re}\frac{\partial u}{\partial y} - uv\right)\right] dV , \\ \displaystyle\int_V \frac{\partial v}{\partial t} dV = -\int_V \frac{\partial p}{\partial y} dV + \int_V \left[\frac{\partial}{\partial x}\left(\frac{1}{Re}\frac{\partial v}{\partial x} - uv\right) + \frac{\partial}{\partial y}\left(\frac{1}{Re}\frac{\partial v}{\partial y} - v^2\right)\right] dV , \\ \displaystyle\int_V \left(\frac{\partial u}{\partial x} + \frac{\partial v}{\partial y}\right) dV = 0 . \end{cases} \tag{3}$$

Applying the Green's Theorem in Eq. (3), results in:

$$\begin{cases} \displaystyle\int_V \frac{\partial u}{\partial t} dV = -\int_V \frac{\partial p}{\partial x} dV + \oint_S \left[\left(\frac{1}{Re}\frac{\partial u}{\partial x} - u^2\right) dy - \left(\frac{1}{Re}\frac{\partial u}{\partial y} - uv\right) dx\right] , \\ \displaystyle\int_V \frac{\partial v}{\partial t} dV = -\int_V \frac{\partial p}{\partial y} dV + \oint_S \left[\left(\frac{1}{Re}\frac{\partial v}{\partial x} - uv\right) dy - \left(\frac{1}{Re}\frac{\partial v}{\partial y} - v^2\right) dx\right] , \\ \displaystyle\int_V \left(\frac{\partial u}{\partial x} + \frac{\partial v}{\partial y}\right) dV = 0 . \end{cases} \tag{4}$$

Considering that the control volume V does not depend on the time, therefore Eq. (4) can

be written as:

$$\begin{cases} \dfrac{\partial u}{\partial t} = -\dfrac{1}{V}\displaystyle\int_V \frac{\partial p}{\partial x} dV + \frac{1}{V}\oint_S \left[\left(\frac{1}{Re}\frac{\partial u}{\partial x} - u^2 \right) dy - \left(\frac{1}{Re}\frac{\partial u}{\partial y} - uv \right) dx \right] , \\ \dfrac{\partial v}{\partial t} = -\dfrac{1}{V}\displaystyle\int_V \frac{\partial p}{\partial y} dV + \frac{1}{V}\oint_S \left[\left(\frac{1}{Re}\frac{\partial v}{\partial x} - uv \right) dy - \left(\frac{1}{Re}\frac{\partial v}{\partial y} - v^2 \right) dx \right] , \\ \displaystyle\int_V \left(\frac{\partial u}{\partial x} + \frac{\partial v}{\partial y} \right) dV = 0 , \end{cases} \tag{5}$$

that it is the integral formulation of the Navier-Stokes equations used for the Finite Volumes method.

3 Projection method

Different methods have been used to solve the incompressible Navier-Stokes equations, expressed in primitive variable form. The Meshless and Finite Differences methods were used to solve Eq. (1) and the Finite Volumes for Eq. (5). The projection method [15] assumes that the velocity field $\mathbf{u}(\mathbf{x}, t_n)$ is known and that the boundary conditions for velocity and pressure are given. The velocity and pressure fields at time $t = t_n + \delta t$ are calculated as follows. Let $\widetilde{p}(\mathbf{x}, t_n)$ be an initial pressure field. Inserting $\widetilde{p}(\mathbf{x}, t_n)$ into Eq. (1) a tentative velocity field $\widetilde{u}(\mathbf{x}, t_n)$ is computed from

$$\begin{cases} \dfrac{\partial \widetilde{u}}{\partial t} + u\dfrac{\partial u}{\partial x} + v\dfrac{\partial u}{\partial y} = -\dfrac{\partial \widetilde{p}}{\partial x} + \dfrac{1}{Re}\left(\dfrac{\partial^2 u}{\partial x^2} + \dfrac{\partial^2 u}{\partial y^2} \right) , \\ \dfrac{\partial \widetilde{v}}{\partial t} + u\dfrac{\partial v}{\partial x} + v\dfrac{\partial v}{\partial y} = -\dfrac{\partial \widetilde{p}}{\partial y} + \dfrac{1}{Re}\left(\dfrac{\partial^2 v}{\partial x^2} + \dfrac{\partial^2 v}{\partial y^2} \right) , \end{cases} \tag{6}$$

with $\widetilde{\mathbf{u}}(\mathbf{x}, t_n) = \mathbf{u}(\mathbf{x}, t_n)$ using the appropriate boundary conditions for $\widetilde{\mathbf{u}}(\mathbf{x}, t_n)$ at $t = t_n$. Equation (6) is solved by a Meshless method or by an explicit Finite Differences method. Let $\mathbf{u}(\mathbf{x}, t_n)$ be defined by

$$\mathbf{u}(\mathbf{x}, t) - \widetilde{\mathbf{u}}(\mathbf{x}, t) = -\nabla\psi(\mathbf{x}, t) \tag{7}$$

where $\psi(\mathbf{x}, t)$ is a function having the property

$$\nabla^2\psi(\mathbf{x}, t) = \nabla \cdot \widetilde{\mathbf{u}}(\mathbf{x}, t) . \tag{8}$$

This linear system is solved by the Bi-conjugated Gradient Stabilized procedure [2]. This iterative method solves linear systems when the matrix is non-symmetric and non-positive definite, just as is the case for Meshless points, that are random, and for the Finite Volumes mesh, that are unstructured.

Now, $\mathbf{u}(\mathbf{x}, t_n)$ conserves mass and possesses the correct vorticity at time t. An equation for pressure is obtained by subtracting Eq. (1) from Eq. (6):

$$\frac{\partial}{\partial t}\left(\mathbf{u} - \widetilde{\mathbf{u}}\right) = -\nabla(p(\mathbf{x}, t) - \widetilde{p}(\mathbf{x}, t_n)). \tag{9}$$

Introducing Eq. (7) into Eq. (9) it yields:

$$-\frac{\partial}{\partial t}\nabla\psi(\mathbf{x}, t) = -\nabla(p(\mathbf{x}, t) - \widetilde{p}(\mathbf{x}, t_n)) \tag{10}$$

and interchanging the operators in Eq. (10) it is obtained:

$$p(\mathbf{x}, t) = \widetilde{p}(\mathbf{x}, t) + \frac{\partial}{\partial t}\psi(\mathbf{x}, t)$$

which is evaluated as:

$$p(\mathbf{x}, t) = \widetilde{p}(\mathbf{x}, t) + \frac{\psi(\mathbf{x}, t)}{\delta t}\ . \tag{11}$$

Therefore Eq. (6), Eq. (8), Eq. (7), and Eq. (11), respectively, must to be solved to simulate the flow. The derivatives in the Finite Differences were calculated using the second order approximation. The convective terms were calculated using the second order upwind method VONOS, see [33].

4 Time step control

It is used by all methods studied here a control procedure to time step at each computational cycle. This procedure [9] is based on the stability restriction bellow:

$$\Delta t \leq \zeta \left[\frac{|u|_{max}}{\Delta x} + \frac{|v|_{max}}{\Delta y} + Re\left(\frac{2}{\Delta x^2} + \frac{2}{\Delta y^2}\right)\right]^{-1}.$$

$\zeta \in (0, 1)$ is the factor employed as a security of the stability. More details can be found in [5]. In this work, $\zeta = 0.5$ was used in all cases.

5 Meshless method

Several methods to Meshless approximations were proposed for various applications. For instance, the Smoothed Particle Hydrodynamics (SPH) is given in Reference [12], Reproducing Kernel Particle Method (RKPM) in Reference [18], Diffuse Element Method (DEM) in Reference [25], Element Free Galerkin Method (EFG) in Reference [4] and Partition of Unity Finite Element Method (PUFEM) in Reference [23]. In the present work, the interest is in Meshless

collocation methods using radial basis functions [10] to approximate regular solutions for systems of equations with linear differential or integral operators. The derivatives in the Meshless method are calculated using this formulation, see [10, 11]. It considers

$$V_I(\mathbf{x}) = c_1(x - x_I)^2 + c_2(x - x_I)(y - y_I) + c_3(y - y_I)^2 + c_4(x - x_I) + c_5(y - y_I) + c_6 \ . \quad (12)$$

It can be observed that when $\mathbf{x} = I$ then $c_6 = V_I$ in Eq. (12), therefore this function can be used to interpolate an I-point property using its neighborhood. The values $c_1, ..., c_5$ can be determined by the Least Square method. It considers

$$\left.\begin{array}{l} \xi = x - x_I \\ \eta = y - y_I \\ V_I(\mathbf{x}) = f \end{array}\right\} \Rightarrow \quad f(\xi, \eta) = c_1\xi^2 + c_2\xi\eta + c_3\eta^2 + c_4\xi + c_5\eta \ . \quad (13)$$

By the Least Square method $\wp(\mathbf{x}) = g_1\alpha_1 + g_2\alpha_2 + g_3\alpha_3 + g_4\alpha_4 + g_5\alpha_5$. The last equation compared with Eq. (13) leads to

$$g_1 = \xi^2, \qquad g_2 = \xi\eta, \qquad g_3 = \eta^2, \qquad g_4 = \xi, \qquad g_5 = \eta \ . \quad (14)$$

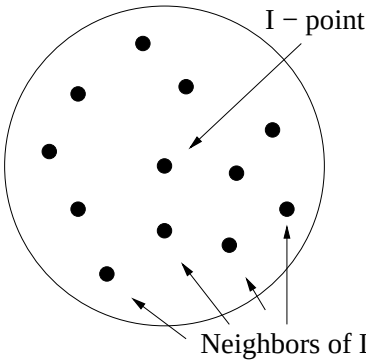

Figure 1: Neighbors of I-point.

Thus, it is necessary to solve the linear system $\mathbf{Ac} = \mathbf{b}$ to find the value of the constants $c_1, ..., c_5$. The matrix $\mathbf{A}$ and the vector $\mathbf{b}$ of this system are given by:

$$A_{ij} = \sum_{k=1}^{m} g_j(x_k)g_i(x_k) \quad \text{and} \quad b_i = \sum_{k=1}^{m} f(x_k)g_i(x_k) \ , \quad (15)$$

where m is the number of neighbors of I, according to Fig. 1. Equation (15) can be expanded

resulting in:

$$\mathbf{A} = \begin{bmatrix} <\xi^2,\xi^2>_k & <\xi^2,\xi\eta>_k & <\xi^2,\eta^2>_k & <\xi^2,\xi>_k & <\xi^2,\eta>_k \\ <\xi\eta,\xi^2>_k & <\xi\eta,\xi\eta>_k & <\xi\eta,\eta^2>_k & <\xi\eta,\xi>_k & <\xi\eta,\eta>_k \\ <\eta^2,\xi^2>_k & <\eta^2,\xi\eta>_k & <\eta^2,\eta^2>_k & <\eta^2,\xi>_k & <\eta^2,\eta>_k \\ <\xi,\xi^2>_k & <\xi,\xi\eta>_k & <\xi,\eta^2>_k & <\xi,\xi>_k & <\xi,\eta>_k \\ <\eta,\xi^2>_k & <\eta,\xi\eta>_k & <\eta,\eta^2>_k & <\eta,\xi>_k & <\eta,\eta>_k \end{bmatrix}, \tag{16}$$

$$\mathbf{b} = \begin{bmatrix} <f,\xi^2>_k \\ <f,\xi\eta>_k \\ <f,\eta^2>_k \\ <f,\xi>_k \\ <f,\eta>_k \end{bmatrix}. \tag{17}$$

where

$$<\zeta,\gamma>_k = \sum_{k=1}^{m} W_k(\xi,\eta)\zeta_k\gamma_k \quad \text{and} \quad W_k(\xi,\eta) = e^{-5\sqrt{\xi^2+\eta^2}}.$$

The function $W_k(\xi,\eta)$ is the exponential weight function, according to Fig. 2. Equation (13) determines that:

$$\begin{cases} \left.\dfrac{\partial f}{\partial x}\right|_I = \left.\dfrac{\partial f}{\partial \xi}\right|_{\substack{\xi=0\\ \eta=0}} = c_4\ , \\ \left.\dfrac{\partial f}{\partial y}\right|_I = \left.\dfrac{\partial f}{\partial \eta}\right|_{\substack{\xi=0\\ \eta=0}} = c_5\ , \\ \left.\dfrac{\partial^2 f}{\partial x^2}\right|_I = \left.\dfrac{\partial^2 f}{\partial \xi^2}\right|_{\substack{\xi=0\\ \eta=0}} = 2c_1\ , \\ \left.\dfrac{\partial^2 f}{\partial y^2}\right|_I = \left.\dfrac{\partial^2 f}{\partial \eta^2}\right|_{\substack{\xi=0\\ \eta=0}} = 2c_3\ , \\ \left.\dfrac{\partial^2 f}{\partial x\partial y}\right|_I = \left.\dfrac{\partial^2 f}{\partial \xi\partial \eta}\right|_{\substack{\xi=0\\ \eta=0}} = c_2\ . \end{cases} \tag{18}$$

The derivatives defined by Eq. (18) are used to discretizate the governing equations.

6 Finite Volumes method

The Finite Volumes method is a numerical method for solving partial differential equations that calculates the values of the conserved variables averaged across the volume. One advantage of the

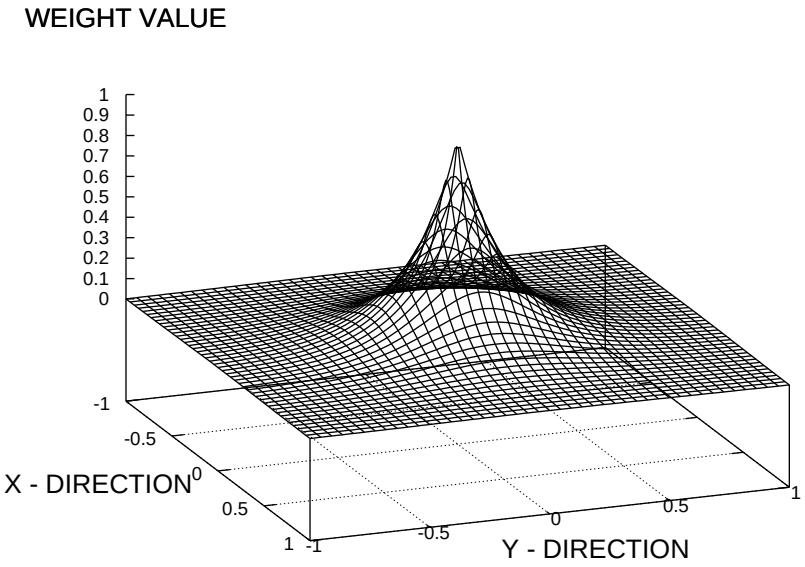

Figure 2: Weight function used in the Meshless method.

Finite Volumes method over Finite Differences method is that it does not require a structured mesh (although a structured mesh can also be used). Furthermore, the Finite Volumes method is preferable to other methods as a result of the fact that boundary conditions can be applied noninvasively. This is true because the values of the conserved variables are located within the volume element, and not at nodes or surfaces. The Finite Volumes method is especially powerful on nonuniform coarse grids and in calculations where the mesh moves to track interfaces or shocks [34].

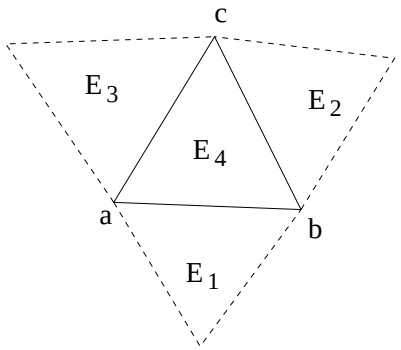

Figure 3: Finite Volumes Cell.

In the Finite Volumes method, the surface integral into momentum equation, given by Eq.

(5), is evaluated in the control volume of Fig. 3. It considers:

$$E_x = \frac{1}{Re}\frac{\partial u}{\partial x} - u^2 \ , \quad F_x = \frac{1}{Re}\frac{\partial u}{\partial y} - uv \ , \quad E_y = \frac{1}{Re}\frac{\partial v}{\partial x} - uv \ , \quad F_y = \frac{1}{Re}\frac{\partial v}{\partial y} - v^2 \ ,$$

then:

$$\oint_S \left[\left(\frac{1}{Re}\frac{\partial u}{\partial x} - u^2\right)dy - \left(\frac{1}{Re}\frac{\partial u}{\partial y} - uv\right)dx\right] = \oint_S E_x dy - \oint_S F_x dx \ ,$$
$$\oint_S \left[\left(\frac{1}{Re}\frac{\partial v}{\partial x} - uv\right)dy - \left(\frac{1}{Re}\frac{\partial v}{\partial y} - v^2\right)dx\right] = \oint_S E_y dy - \oint_S F_y dx \ ,$$

where

$$\oint_S E dy\bigg|_{E_4} \approx \frac{1}{2}\left[(E_4 + E_1)dy_{ab} + (E_4 + E_2)dy_{bc} + (E_4 + E_3)dy_{ca}\right] \ ,$$
$$\oint_S F dx\bigg|_{E_4} \approx \frac{1}{2}\left[(F_4 + F_1)dx_{ab} + (F_4 + F_2)dx_{bc} + (F_4 + F_3)dx_{ca}\right] \ .$$

In E_4 appears the derivative $\frac{\partial u}{\partial x}$, that is approximated by:

$$\frac{\partial u}{\partial x}\bigg|_{E_4} \approx \frac{1}{V}\int_V \frac{\partial u}{\partial x} dV = \frac{1}{V}\oint_S u dy$$
$$\approx \frac{1}{2V}\left[(u_4 + u_1)dy_{ab} + (u_4 + u_2)dy_{bc} + (u_4 + u_3)dy_{ca}\right] \ .$$

For $\frac{\partial u}{\partial y}$ and E_1, E_2 and E_3, the procedure is analogous.

7 Driven cavity problem

In the driven cavity problem, the flow is induced by a sliding motion of the top wall $y = 1$ from left to right. It is described by the Navier-Stokes Eq. (1), for the Finite Differences and Meshless methods, and Eq. (5), for the Finite Volumes method.

The boundary conditions are no-slip Dirichlet type for the velocity field. On the stationary walls $u = 0$ and $v = 0$. On the sliding wall $u = 1$ and $v = 0$, according to Fig. 4a. The boundary conditions to the pressure field are Neumann type $\frac{\partial p}{\partial n} = 0$, where n is the normal direction to the cavity wall.

In the left bottom corner, it was considered one Dirichlet condition for the pressure: $p = 0$. This was done to assure that the matrix of linear system, in the pressure calculus, does not become singular. This does not affect the results because the pressure variation is more important, see Eq. (8).

The Neumann conditions, in the Finite Volumes and Meshless methods, are assured by the reflection nodes technique. That it was applied near to the stationary walls and the sliding wall. In the Meshless method, a node band equal to the influence radius of the neighborhood was used.

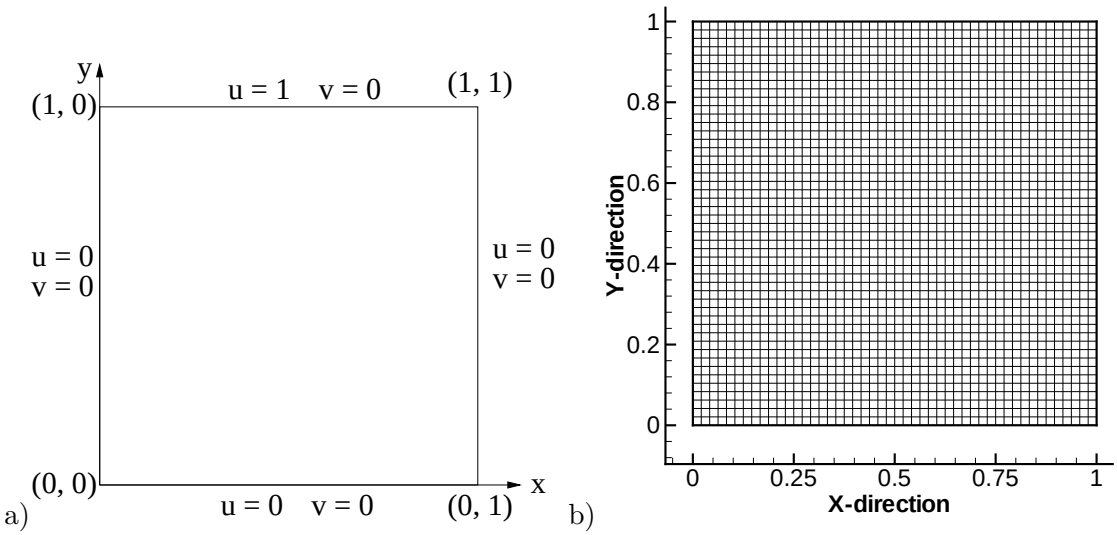

Figure 4: a) Cavity Problem and b) Finite Differences Mesh.

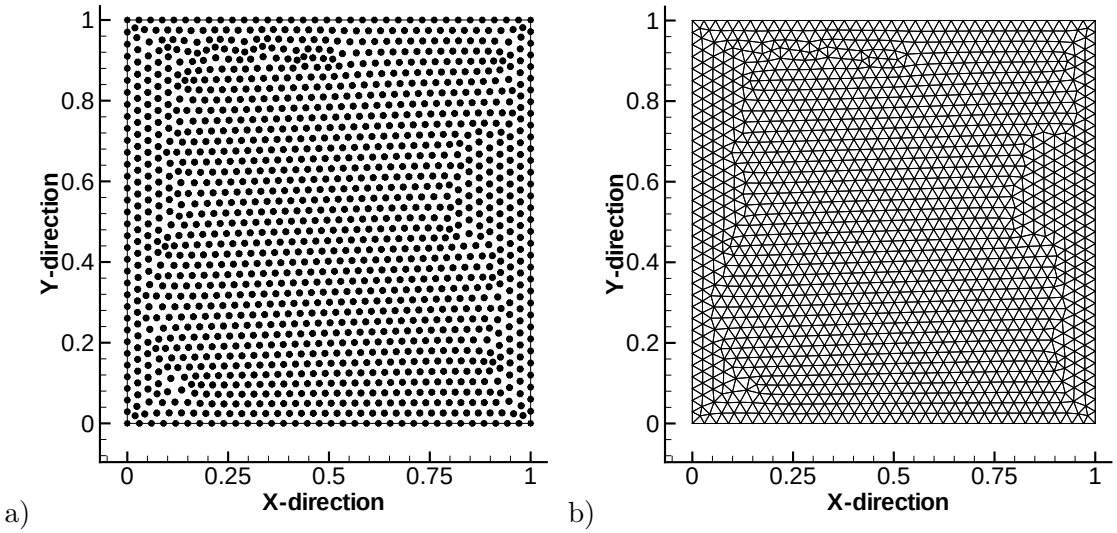

Figure 5: a) Meshless Points and b) Finite Volumes Mesh

8 Results

All methods were solved using C^{++} programming language implemented in a generic i386 Linux platform. The results to the Meshless method were obtained using the points showed by Fig. 5a. The mesh showed in the Fig. 5b was used by the Finite Volumes method. The Finite Differences method used a 50×50 grid, showed by Fig. 4b.

Figure 6-8 shows the streamlines in the cavity for the Finite Differences, Meshless and Finite Volumes methods. In the results showed in Fig. 6 to 8, $Re = 0.1$, 10, 50 and 100. Figures 9 and 10 show the u-velocity distribution along a horizontal line ($y = 0.5$) and u-velocity along a vertical line ($x = 0.5$) respectively. Figures 11 and 12 show the v-velocity distribution along a horizontal line ($y = 0.5$) and v-velocity along a vertical line ($x = 0.5$) respectively, at various Reynolds numbers.

The graphics shown in Fig. 9 to 12 were plotted using a node band around the cavity centerlines, because the nodes of unstructured mesh do not coincide with the nodes of structured mesh. This procedure prevent mesh interpolations. Tables 1 and 2 were assembled using the results of u-velocity and v-velocity in the horizontal and vertical centerlines.

The precision was calculated using:

$$\varepsilon_{fv} = \frac{\| |\sigma^{fd}| - |\sigma^{fv}| \|_p}{\|\sigma^{fd}\|_p} \quad \text{and} \quad \varepsilon_m = \frac{\| |\sigma^{fd}| - |\sigma^{m}| \|_p}{\|\sigma^{fd}\|_p} \ .$$

where ε_{fv} and ε_m are the errors of the Finite Volumes and Meshless methods compared to the Finite Differences method and σ is the u-velocity or v-velocity vectors. It was used L^5 and L^∞ norms defined as:

$$\|\mathbf{x}\|_5 = \left(\sum_{r=1}^{n} |x_r|^5 \right)^{\frac{1}{5}} ,$$
$$\|\mathbf{x}\|_\infty = \max_{1 \le r \le n} |x_r| \ .$$

Table 3 shows the primary vortex center for the Finite Differences, Finite Volumes and Meshless methods and the data of Reference [31] for $Re = 1$ and $Re = 100$. Table 4 presents a comparative u and v-velocity in horizontal centerline ($y = 0.5$) for $Re = 100$ and Tab. 5 presents a comparative u and v-velocity in vertical centerline ($x = 0.5$) for $Re = 100$.

Table 1: Comparative error table in horizontal centerline at y=0.5.

Re	L^∞-norm				L^5-norm			
	u-velocity		v-velocity		u-velocity		v-velocity	
	ε_{fv}	ε_m	ε_{fv}	ε_m	ε_{fv}	ε_m	ε_{fv}	ε_m
0.1	0.06933	0.15256	0.15161	0.17906	0.05895	0.15376	0.11556	0.16058
1.0	0.06875	0.15255	0.15108	0.17839	0.05848	0.15377	0.11523	0.16030
10.0	0.06314	0.09118	0.14424	0.16987	0.05398	0.09044	0.10968	0.13104
25.0	0.05400	0.08113	0.13928	0.16562	0.04659	0.08193	0.10604	0.12775
50.0	0.03980	0.07328	0.11294	0.14991	0.03502	0.07966	0.08542	0.10881
100.0	0.03373	0.12049	0.11839	0.24242	0.02623	0.12297	0.09737	0.20029
Mean	0.05479	0.11186	0.13625	0.18087	0.04654	0.11375	0.10488	0.14812

Table 2: Comparative error table in vertical centerline at x=0.5.

Re	L^∞-norm				L^5-norm			
	u-velocity		v-velocity		u-velocity		v-velocity	
	ε_{fv}	ε_m	ε_{fv}	ε_m	ε_{fv}	ε_m	ε_{fv}	ε_m
0.1	0.06689	0.04191	0.00725	0.00966	0.05980	0.05839	0.00856	0.01121
1.0	0.06684	0.04190	0.00709	0.01046	0.05975	0.05838	0.00835	0.01134
10.0	0.06641	0.02089	0.02182	0.02433	0.05938	0.02506	0.02527	0.03150
25.0	0.06645	0.02305	0.02037	0.03650	0.05950	0.02429	0.02387	0.03696
50.0	0.06912	0.02275	0.01729	0.04668	0.06231	0.02679	0.02053	0.04372
100.0	0.07905	0.06303	0.01474	0.06069	0.07229	0.06243	0.01835	0.05631
Mean	0.06912	0.03558	0.01476	0.03138	0.06217	0.04222	0.01748	0.03184

Table 3: Location of primary vortex center.

Reynolds Number	Finite Differences		Finite Volumes		Meshless		Schreiber & Keller	
	x	y	x	y	x	y	x	y
0.1	0.4883	0.7624	0.4978	0.7638	0.5020	0.7430	-	-
1	0.4906	0.7624	0.4998	0.7631	0.5032	0.7427	0.5	0.76667
10	0.5045	0.7614	0.5060	0.7623	0.5183	0.7538	-	-
25	0.5299	0.7591	0.5391	0.7608	0.5437	0.7557	-	-
50	0.5691	0.7582	0.5714	0.7614	0.5767	0.7553	-	-
100	0.6107	0.7338	0.6130	0.7407	0.6306	0.7434	0.61667	0.74167

Table 4: Comparative u-velocity and v-velocity table in horizontal centerline at y=0.5 for $Re = 100$.

Position	Finite Differences		Finite Volumes		Meshless	
	u_x	v_x	u_x	v_x	u_x	v_x
0.25	-0.096871	0.178925	-0.092850	0.174070	-0.081806	0.151773
0.5	-0.207203	0.0518048	-0.206589	0.057071	-0.180446	0.057445
0.75	-0.211439	-0.233569	-0.210336	-0.229064	-0.190579	-0.191401

Table 5: Comparative u and v velocities table in vertical centerline at x=0.5 for $Re = 100$.

Position	Finite Differences		Finite Volumes		Meshless	
	u_y	v_y	u_y	v_y	u_y	v_y
0.25	-0.146992	-0.00114387	-0.141713	0.002462	-0.119133	0.006843
0.5	-0.207203	0.0518048	-0.206329	0.058145	-0.179992	0.057980
0.75	0.036096	0.108712	0.023795	0.119201	0.020259	0.120330

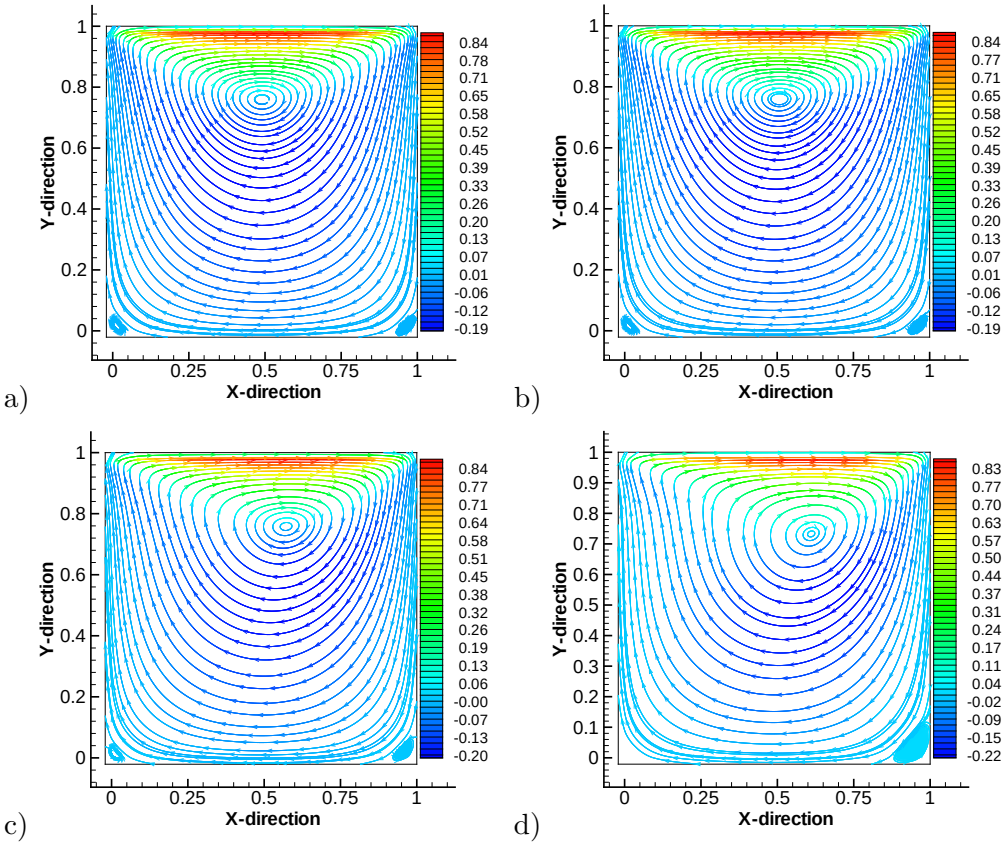

Figure 6: Finite Differences: a) $Re = 0.1$, b) $Re = 10$, c) $Re = 50$ and d) $Re = 100$.

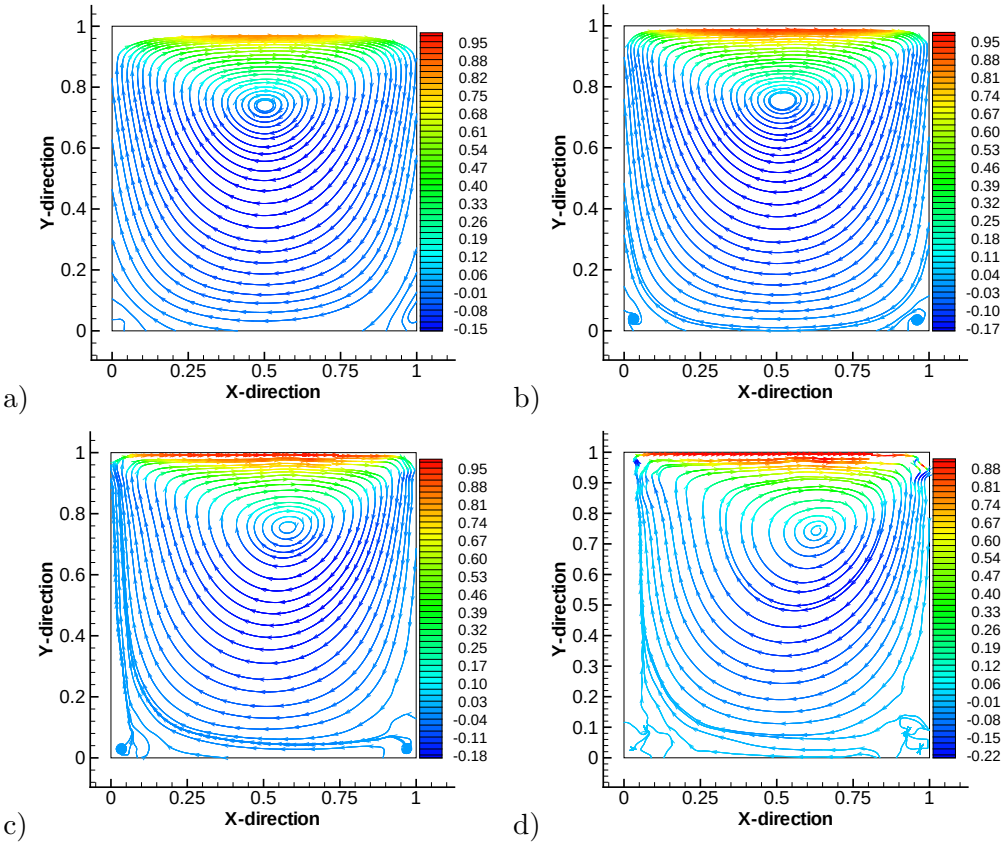

Figure 7: Meshless: a) $Re = 0.1$, b) $Re = 10$, c) $Re = 50$ and d) $Re = 100$.

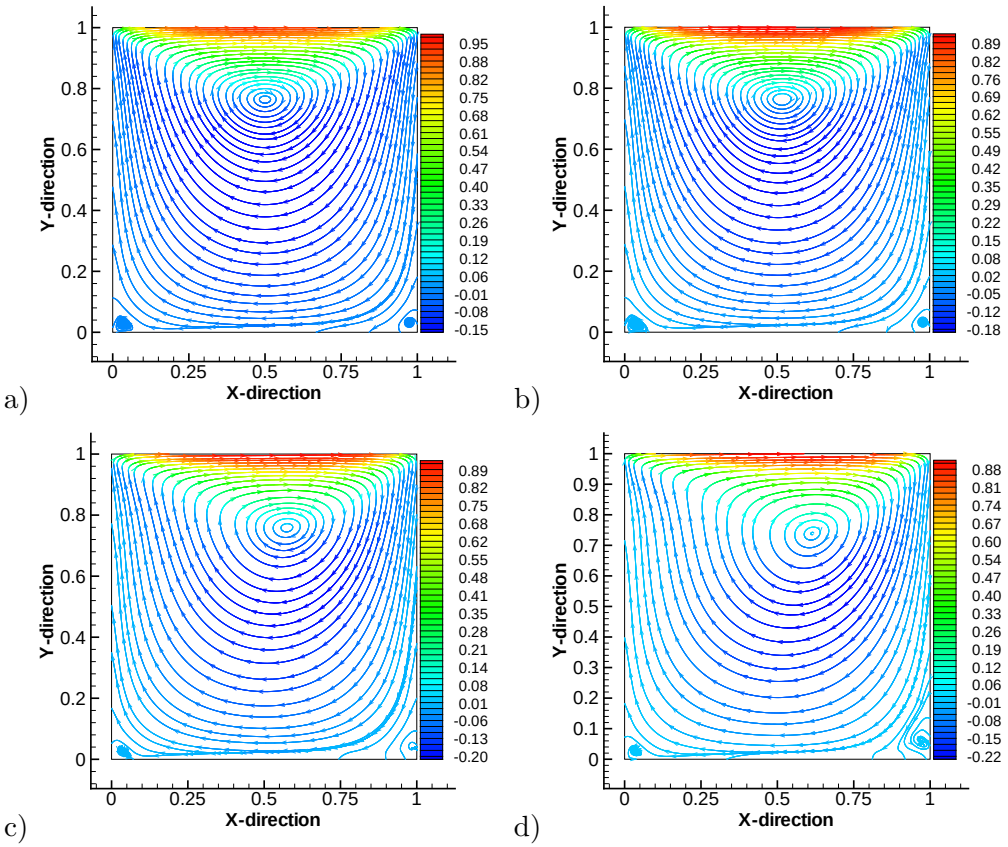

Figure 8: Finite Volumes: a) $Re = 0.1$, b) $Re = 10$, c) $Re = 50$ and d) $Re = 100$.

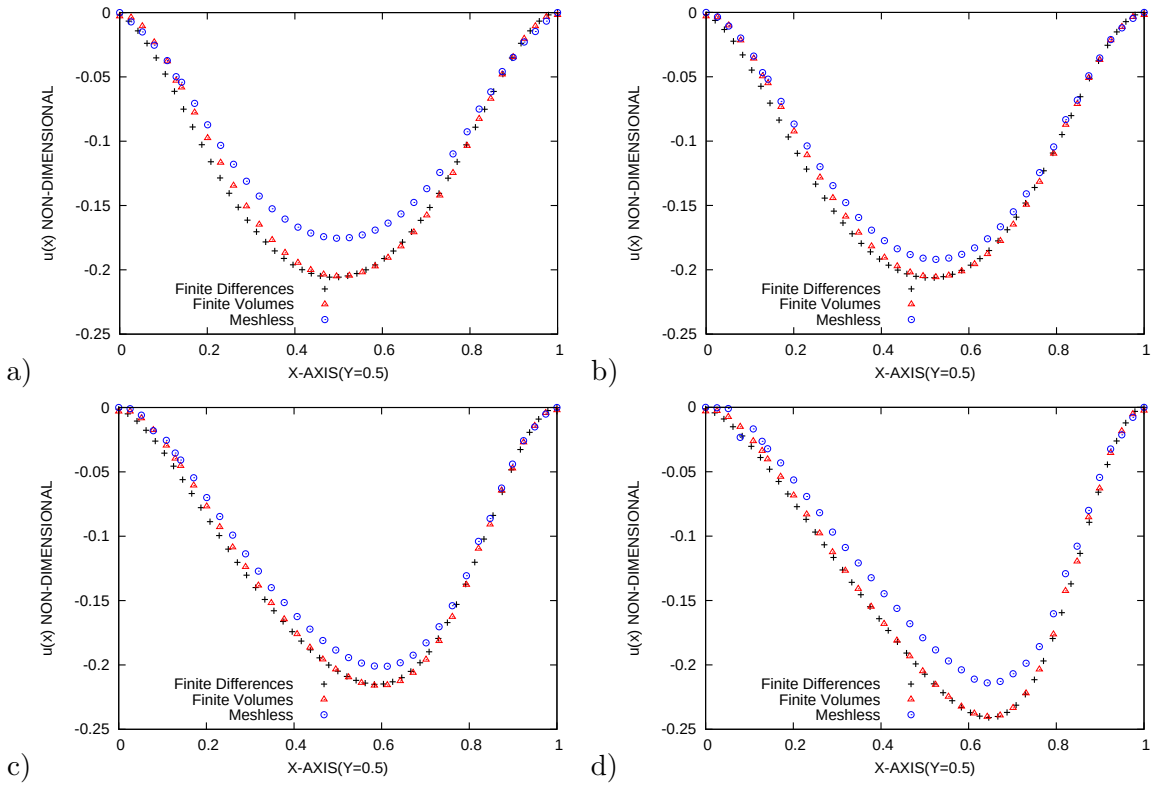

Figure 9: Horizontal centerline for u at $y = 0.5$: a)$Re = 0.1$ b)$Re = 10$ c)$Re = 50$ d)$Re = 100$.

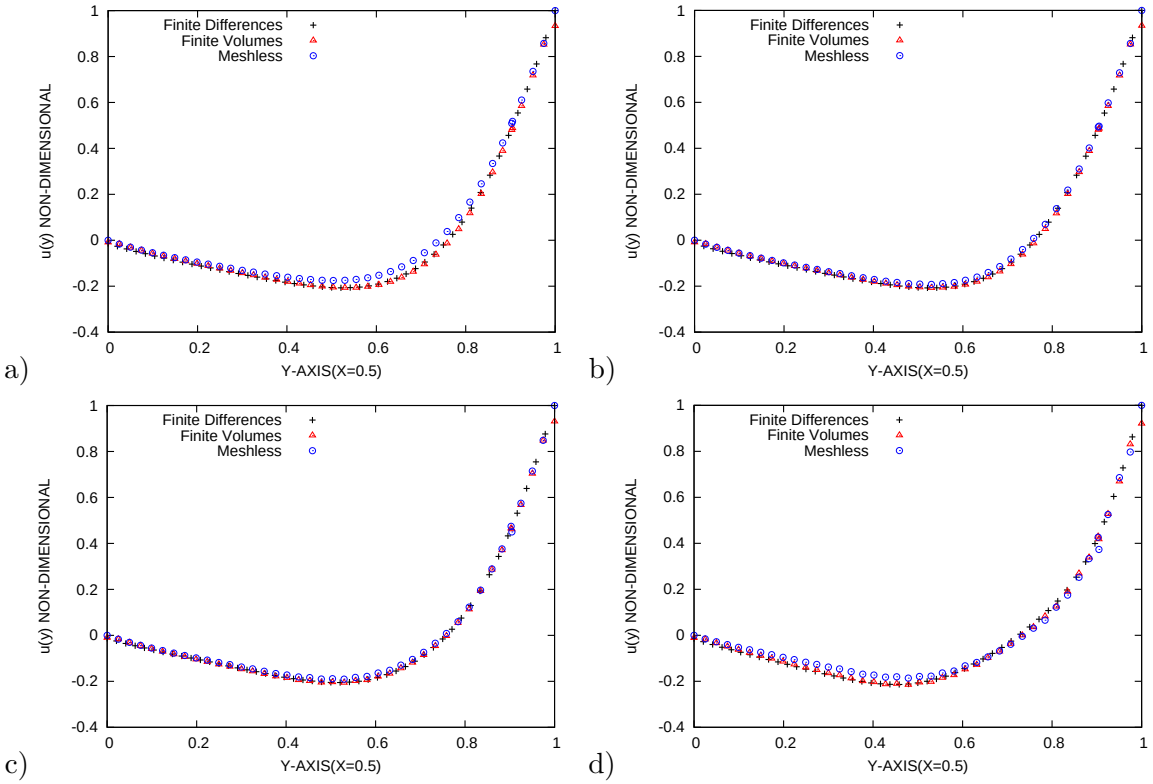

Figure 10: Vertical centerline for u at $x = 0.5$: a)$Re = 0.1$ b)$Re = 10$ c)$Re = 50$ d)$Re = 100$.

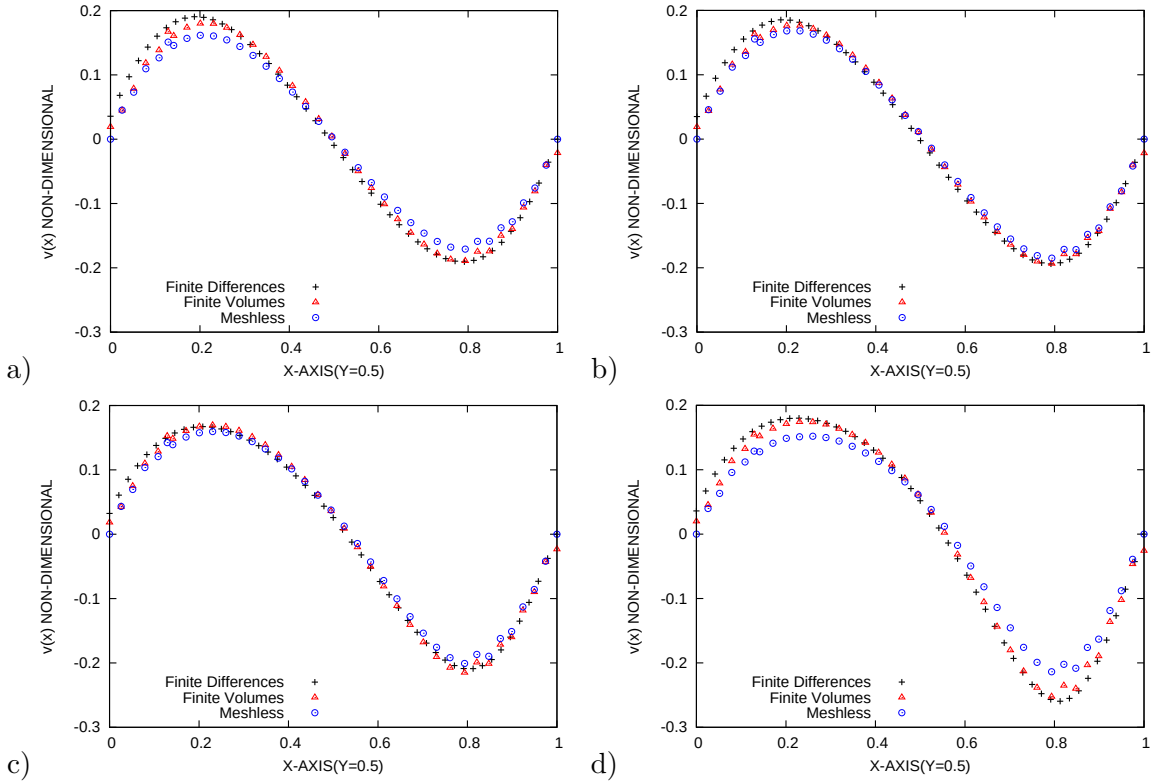

Figure 11: Horizontal centerline for v at $y = 0.5$: a)$Re = 0.1$ b)$Re = 10$ c)$Re = 50$ d)$Re = 100$.

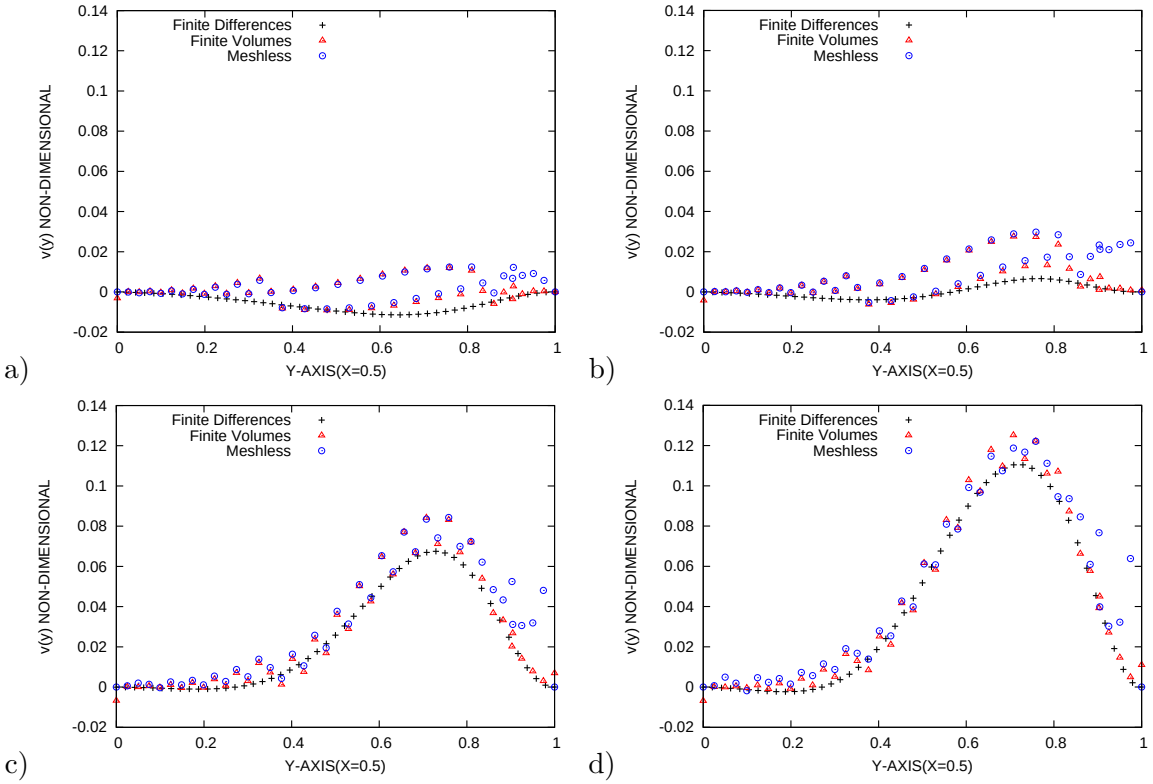

Figure 12: Vertical centerline for v at $x = 0.5$: a)$Re = 0.1$ b)$Re = 10$ c)$Re = 50$ d)$Re = 100$.

9 Discussions

The position of the primary vortex center with the data of Reference [31] was compared in order to verify if the numerical methods used were solving correctly the cavity flow problem. The flow generated in a fluid-filled square cavity due the uniform translation of one wall of the cavity (sliding wall) represents one of the simplest examples of steady flow involving closed streamlines. Many researchers have been studied this model with theoretical arguments, quantitative measurements, qualitative measurements and many others methods. It is worth pointing that the flow behavior in a cavity has viscous and inertial forces that will produce the recirculation of the flow inside of the driven cavity.

The streamline plots (see Fig. 6 to 8) show the formation of a primary vortex (nearly circular and central) whose center is displaced in direction x and to top. This streamlines indicates that there are secondary vortexes that do not shrink significantly when Reynolds number grows.

In the graphics shown in Fig. 9 to Fig. 12 it can be observed that the Finite Differences and Finite Volumes methods present results very closed. The results are in good agreement

with [32] and [29]. Numerical experiments indicate that the Meshless formulation can provide higher accuracy in comparison with the standard re-meshing used with viscous scheme, [3]. However the present results show an artificial dissipation that is more evident at low Reynolds numbers.

It can be seen in Fig. 6 to Fig. 8 that the Meshless method are not precise in capture the vorticity in the bottom corners (secondary vortex) of the driven cavity. This comparisons indicate that the profiles agreed well one with the other, except for some discrepancies near the left and right bottom corners of the cavity in the Meshless solution.

In the neighborhood of those singular points (corners), the Meshless algorithm looses precision because of the imposition of the ghost points to approximate the boundary condition (Neumann condition). In those points a discontinuity associated with the ghost band points in the exterior of the cavity generated by the reflection method exist. This discontinuities are mentioned by [6,13]. When the value of the Reynolds number increases, the inadequacy of coarse meshes gradually becomes apparent. This would imply that the velocity distributions near the corners are also sensitive to the mesh size.

The reason why it was chosen to plot the u and v-velocities profiles is to test the accuracy of the solution comparing one with the other and with others authors also [7, 21, 24, 31]. The results obtained in this study show more accuracy for the Finite Volumes method followed by the Meshless method compared with the Finite Differences method.

It can be observed in Tab. 1 and 2 that, as an average, the Finite Volumes method gives a better approximation compared with the Finite Differences method that the Meshless method. This occurs because the error increases where there are more transport of fluid and numerical diffusivity. In the Meshless method the choice of neighbors influence radius and the weight function are directly related with this fact. However it remains the problem of discontinuity in the boundary corners.

It can be seen that the flow feature is a function of the position along the span of cavity (see Fig. 9 to Fig. 12). However the magnitude of the variations appears to be related to the Reynolds number. They are different between the symmetry and end-wall planes. But they are not significantly different for $Re = 1$ and $Re = 10$.

The flow exhibits global and local features. As for the global features, the flow appears to manifest itself as an adjustment to the shear gradients resulting from the presence of end-walls and the boundary conditions. In the local feature, the flow contains the primary vortex and corner notices along the end-walls, which depends mainly of the Reynolds number.

It can be noted that with the reduction of the viscous effects there are reduction of the error in u and v velocities components in the horizontal centerline of driven cavity. In the vertical centerline the error increases with the reduction of the viscous effects in the u and v velocities components, for the Meshless and Finite Volumes methods. This can be explained by the fact that in the vertical centerline of the driven cavity there are less fluid transport than in the horizontal centerline.

The numerical simulation produced significantly different velocity profiles in horizontal and

vertical centerlines, because the centerline does not cross the center of the primary vortex. In addition, the velocity fluctuations in the vertical direction are significantly higher than those in the horizontal direction.

In this computations, Tab. 4 and 5 show the velocities u and v at 0.25, 0.5 and 0.75 distance in horizontal and vertical centerlines. Numerically, the results are coherent with the standard one by Finite Differences.

Concerning the accuracy of the results of Tab. 3, it can be concluded that the data on the primary vortex are correct within 2%. This was concluded comparing the results of [31] for $Re = 1$ and $Re = 100$.

The advantages or disadvantages of these numerical approaches, the numerical stability and any type of the numerical features are not target in this work. The discrepancies near the left and right hand side of the driven cavity corners will be study with new solutions strategies of boundary conditions and numerical approach. The present results should be very useful and we intend to study this methods for meshes with more points near the boundary and few points in the center of the cavity.

The 2-D steady incompressible driven cavity flow can to serve as a model flow problem and a good benchmark problem for different numerical methods in terms of accuracy, convergence rate, boundary conditions, etc. There is much here for discussion and improvement.

Future effort includes consideration of primitive-variable formulation when applied for higher Reynolds numbers and scattered mesh. Better and quick solution will be possible with use of the Multigrid techniques to accelerate the convergence of the linear system solver.

References

[1] E. Barragy and G. F. Carey. Stream function-vorticity driven cavity solutions using p finite elements. *Computer and Fluids*, 26:453–468, 1997.

[2] R. Barret, M. Berry, T. F. Chan, J. Demmel, J. Donnato, V. Eijkhout, R. Pozzo, Romine C, and H. Van der Vorst. *Templates for the solution of linear systems: Building blocks for iterative methods.* SIAM, 1994.

[3] T. Belytschko, Y. Krongaus, D. Organ, M. Fleming, and P. Krysl. Meshless methods: An overview and recent developments. *Computational Methods in Applied Mechanics Engineering*, 139:3–47, 1996.

[4] T. Belytschko, Y. Y Lu, and L. Gu. Element-free galerkin methods. *International Journal for Numerical Methods in Engineering*, 37:229–256, 1994.

[5] U. Bulgarelli, V. Casulli, and D. Greenspan. *Pressure methods for numerical solution of free surface fluid flows.* Swansea, Pineridge Press, 1984.

[6] H. J. Choe, D. W. Kim, H. H. Kim, and Y. Kim. Meshless method for the stationary incompressible navier-stokes equations. *Discrete And Continuous Dynamic Systems. Series B*, 1(4):495–526, 2001.

[7] E. Erturk, T. C. Corke, and C. Gakcol. Numerical solutions of 2-d steady incompressible driven cavity flow at high reynolds number. *International Journal for Numerical Methods in Fluids*, 48:747–774, 2004.

[8] C. A. J. Fletcher. *Computational techniques for fluid dynamics*. Springer-Verlag, New York, 1991.

[9] A. O. Fortuna. *Técnicas computacionais para dinâmica dos fluidos: Conceitos básicos e aplicações*. Editora da Universidade de São Paulo, 2000.

[10] C. Franke and R. Schaback. Convergence orders of meshless collocation methods using radial basis functions. *Advances in Computational Mathematics*, 8:381–399, 1998.

[11] R. Franke and G. Nielsen. Smooth interpolation for large sets of scattered data. *International Journal for Numerical Methods in Engineering*, 15:1691–1704, 1980.

[12] R. Gingold and J. Monaghan. Smoothed particle hydrodynamics - theory and application to monospherical stars. *Monthly Notices of the Royal Astronomical Society*, 181:375–, 1977.

[13] F. C. Günther and W. K. Liu. Implementation of boundary conditions for meshless methods. *Computer Methods in Applied Mechanics and Engineering*, 163(1-4):205–230, 1998.

[14] Murli M. Gupta and Jiten C. Kalita. A new paradigm for solving navier-stokes equations: streamfunction-velocity formulation. *Journal of Computational Physics*, 207(1):52–68, 2005.

[15] F. Harlow and J. E. Welch. Numerical calculation of time-dependent viscous incompressible flow of fluid with a free surface. *Physics of Fluids*, 8:2182–2189, 1965.

[16] J. R. Koseff and R. L. Street. The lid-driven cavity flow: A synthesis of qualitative and quantitative observations. *Journal of Fluids Engineering*, 106:390–398, 1984.

[17] J. R. Koseff and R. L. Street. On end wall effects in a lid-driven cavity flow. *Journal of Fluids Engineering*, 106:385–389, 1984.

[18] W. K. Liu, S. Jun, S. Li, J. Adee, and T. Belytschko. Reproducing kernel particle methods for structural dynamics. *International Journal for Numerical Methods in Engineering*, 38(10):1655–1679, 1995.

[19] C. R. Maliska and J. F. V. Vasconcellos. An unstructured finite volume procedure for simulating flows with moving fronts. *Computer Methods in Applied Mechanics and Engineering*, 182(3,4):401–420, 2000.

[20] Clovis R. Maliska. *Transferência de calor e mecânica dos fluidos computacional*. LTC Editora, Rio de Janeiro, 2000.

[21] H. L. Meitz and H. F. Fasel. A compact-difference scheme for the navier-stokes equations in vorticity-velocity formulation. *Journal of Computational Physics*, 157:371–403, 2000.

[22] J. M. Melenk. On approximation in meshless methods. Technical report, ETH-Eidgenössische Technische Hochschule Zürich, 1997.

[23] J. M. Melenk and I. Babuška. The partition of unity finite element method: basic theory and applications. In *Seminar für Angewate Mathematic*, volume 96-01. Eidgenössische Technische Hoschschule, January 1996.

[24] S. Narasimhan. Navier-stokes solution of the driven-cavity problem using sinc-collocation elements. In *32nd AIAA Fluid Dynamics Conference*. AIAA, June 2002.

[25] B. Nayroles, G. Touzot, and P. R. A. Villon. Generalizing the finite element method: diffuse approximation and diffuse elements. *Computational Mechanics*, 10(5):307–318, 1992.

[26] Frank Pan and Andreas Acrivos. Steady flows in rectangular cavities. *Journal of Fluid Mechanics*, 28:643–655, 1967.

[27] G. Pascazio and M. Napolitano. A staggered-grid finite volume method for the vorticity-velocity equations. *Computer & Fluids*, 25(4):433–446, 1996.

[28] J. M. C. Pereira, M. H. Kobayashi, and J. C. F. Pereira. A fourth-order-accurate finite volume compact method for the incompressible navier-stokes solutions. *Journal of Computational Physics*, 167:217–243, 2001.

[29] F. A. Schneider and C. R. Maliska. Uma formulacão em volumes finitos usando malhas não-estruturadas. *VIII ENCIT - Encontro Nacional de Ciências Térmicas*, CD Rom edition, 2000.

[30] F. A. Schneider and C. R. Maliska. Solução numérica simultânea de escoamentos bidimensionais incompressíveis pelo método dos volumes finitos usando malhas não-estruturadas. In *ENCIT-9Th Brazilian Congress of Thermal Engineering and Sciences*, 2002.

[31] R. Schreiber and H. B. Keller. Driven cavity flows by efficient numerical techniques. *Journal of Computational Physics*, 49:310–333, 1983.

[32] B. D. Semeraro and A. Sameh. Solution of the navier-stokes equations for a driven cavity. Technical report, NASA-CR-188008 and Ilinois University, 1991.

[33] A. Varonos and G. Bergeles. Development and assessment of a variable-order non-oscillatory scheme for convection term discretization. *International Journal for Numerical Methods in Fluids*, 26:1–16, 1998.

[34] H. K. Versteeg and W. Malalasekera. *An introduction to computational fluid dynamics. The Finite Volume method*. Prentice Hall, Essex, 1995.